

Low-volume liquid delivery and nanolithography using a nanopipette combined with a quartz tuning fork-atomic force microscope†

Sangmin An,^a Corey Stambaugh,^{‡a} Gunn Kim,^b Manhee Lee,^{§a} Yonghee Kim,^a Kunyoung Lee^a and Wonho Jhe^{*a}

Received 23rd April 2012, Accepted 9th August 2012

DOI: 10.1039/c2nr30972f

Electric-field-induced low-volume liquid ejection under ambient conditions was realized at a low bias potential of 12 V *via* a nanopipette (aperture diameter of 30 nm) combined with a non-contact, distance-regulated (within 10 nm) quartz tuning fork-atomic force microscope. A capillary-condensed water meniscus, spontaneously formed in the tip–substrate nanogap, reduces the ejection barrier by four orders of magnitude, facilitating nanoliquid ejection and subsequent liquid transport/dispersion onto the substrate without contact damage from the pipette. A study of nanofluidics through a free-standing liquid nanochannel and nanolithography was performed with this technique. This is an important breakthrough for various applications in controlled nanomaterial-delivery and selective deposition, such as multicolor nanopatterning and nano-inkjet devices.

Introduction

Nanofluidics is a rapidly emerging research field which addresses the fluidic characteristics of various nanosystems.^{1–4} In particular, the low-volume liquid delivery/patterning based on the fluidics under ambient conditions is very important and has high potential in the field of nanobiotechnology. There has been much effort to realize the delivery of tiny amounts of liquid using nanofluidic devices such as nanopores^{5–7} and nanochannels.^{8–10} The nanopipette,^{11–14} a versatile fluidic tool¹⁵ for sensitive detection,¹⁶ high-resolution imaging,¹⁷ biochemical analysis,¹⁸ controlled delivery^{19,20} and manipulation²¹ of nanomaterials, can be a suitable device for the delivery of low-volume liquids. In addition, it can be easily produced with various aperture sizes (30 nm to 10 μm), unlike other intricately fabricated nanodevices, and it can be readily combined with scanning probe microscopy for nanometric manipulation. However, it is very difficult for the liquid inside the nanopipette to be ejected out of the aperture due to the surface tension under ambient conditions even if the electric field increases by several orders of magnitude. Although jet-printing by using micropipettes is a well-established technique

for microscopic liquid ejection in the air,²² it cannot be directly applied to nanofluidic research because one has to overcome extremely high barriers associated with the surface tension and the atmospheric pressure at the nanoaperture.

Here, we have realized a versatile experimental scheme for nanopipette-based low-volume liquid delivery and nanolithography by employing the nanopipette as the probe tip of a homemade, non-contact, small-amplitude-modulation quartz tuning fork-atomic force microscope (QTF-AFM). The capillary-condensed water nanomeniscus that naturally forms between the apex of the nanopipette and the surface plays a key role in the ejection of the liquid onto the substrate. This novel tool provides several breakthroughs: (i) a substantial lowering of the ejection barrier potential from $\sim 10^5$ V to ~ 10 V *via* the spontaneous formation of the capillary-condensed water nanomeniscus,²¹ (ii) low-field-controlled transport and delivery of the ejected nanoliquids to the substrate through the same water nanomeniscus and (iii) avoidance of mechanical contact damage to the nanopipette, allowing for its repetitive and reliable use.

Methods

Nanopipette

The controlled manipulation and delivery of a small volume of liquid onto a substrate was facilitated by a pencil-shaped, pulled nanopipette, which was fabricated using a commercial puller (P-2000, Sutter Instruments Co.). In general, three materials are used to produce nanopipettes: borosilicate, quartz and aluminosilicate. The borosilicate pipettes were chosen (outer diameter of 1 mm and inner diameter of 0.7 mm) to make smaller apertures and thinner shapes. Furthermore, of the three materials, the

^aDepartment of Physics and Astronomy, Seoul National University, Daehak-dong, Gwanak-gu, Seoul 151-747, Republic of Korea. E-mail: whjhe@snu.ac.kr; Fax: +82 2 886-5786; Tel: +82 2 880-6600

^bDepartment of Physics and Graphene Research Institute, Sejong University, 98 Gunja-Dong, Gwangjin-Gu, Seoul 143-747, Republic of Korea

† Electronic supplementary information (ESI) available. See DOI: 10.1039/c2nr30972f

‡ Present address: National Institute of Standards and Technology, MD 20899, USA.

§ Present address: Department of Physics, Harvard University, Cambridge, MA 02138, USA.

borosilicate nanopipette tip reduced the quality factor of the QTF the least. After pulling, filling of the liquid solution is facilitated *via* the capillary force due to a pre-installed filament inside the glass pipette. The aperture sizes of the nanopipettes can be characterized by a typical resistance-measurement system using an I - V converter (10^7 gain) with an arbitrary 0.1 M NaCl solution (conductivity of $1.068 \Omega \text{ m}$) and by correlating the results with the scanning electron microscopic images (Fig. 1). For example, the electrical resistance of the 30 nm aperture was $35.3 \text{ M}\Omega$ according to our measurement. The aperture size of the pulled nanopipette was controlled by varying the pulling power parameter of the puller (Fig. S-1 in the ESI†).

Combined nanopipette/QTF-AFM

We now discuss the investigation of a field-induced nanofluidic ejection and transport of the liquid through the nanopipette under ambient conditions by employing the standard QTF-AFM.^{23,24} The QTF, which is widely used as a linear force sensor of high-sensitivity,²⁵ is an ideal piezoelectric device for nanometric distance control ($<10 \text{ nm}$) providing information on the tip-substrate separation, with the added advantage that its quality factor is not significantly affected by the attached AFM tip. We employed the non-contact, small-amplitude-modulated ($<1 \text{ nm}$) shear-mode QTF-AFM, operating at $\sim 32\,768 \text{ Hz}$, which provides the stability and controllability needed for the spontaneous formation of the capillary-condensed water nanomeniscus in the nanogap. The general characteristics of this QTF

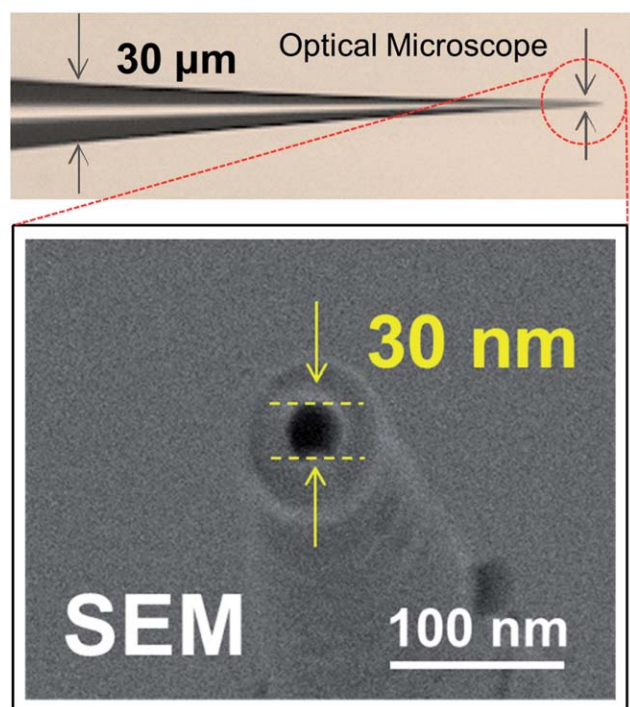


Fig. 1 The pulled nanopipette. An optical microscope (OM) image of a typical pencil-shaped nanoaperture glass pipette fabricated by thermal heating followed by mechanical pulling (P-2000, Sutter Co.) and a scanning electron microscope image of its 30 nm aperture. By changing the pulling parameters, we can produce various aperture sizes (Fig. S-1 in the ESI†).

system are presented in the ESI,† including the viscoelasticity of one-dimensionally confined water nanomeniscuses.^{26,27}

Fig. 2(a) shows a diagram of the capillary-condensed water meniscus formed between the tip and the substrate within 10 nm of the surface, which is the key to the low-volume liquid ejection through an aperture of the pipette that is tens of nanometers in diameter; this is achieved by overcoming the barrier of surface tension under ambient conditions. Fig. 2(b) shows the diagram of our proposed system. The process leading to the ejection of the studied liquids from the nanopipette is outlined as follows. As the tip approaches within 10 nm of the surface, the

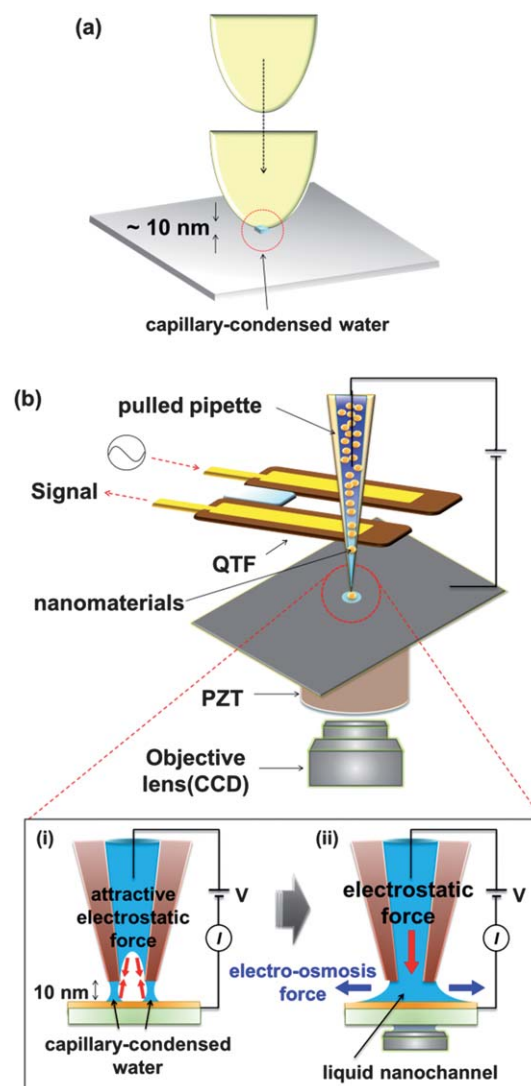


Fig. 2 Low-electric-field-induced nanoscale liquid ejection and transport *via* a nanopipette under ambient conditions. (a) Diagram of the capillary-condensed water (key to the experiment). When the tip approaches the surface, the nanoscale water meniscus can be naturally formed between the tip and the substrate. (b) Schematic of the combined nanopipette/QTF-AFM setup. The experimental procedures consisted of two steps: (i) formation of the capillary-condensed water nanomeniscus during the nanopipette approach within 10 nm of the surface and subsequent application of the electric field, (ii) observation of the resulting ejection, transport and dispersion of the liquids through the liquid nanochannel.

capillary-condensed water nanomeniscus forms in the nanopipette–substrate nanogap in a cylindrically shaped shell around the aperture rim while leaving a cavity within it, and the top edge of the meniscus is separated (by about 1 nm) from the liquid filled inside the pipette. When the small electric potential, which is applied between the electrode inside the nanopipette and the electro-plated substrate, is large enough, an attractive electrostatic force draws the two liquids together.²⁸ This results in the cavity being filled with the liquid of interest, bridging the nanopipette and the substrate and leading to the low-field-induced ejection of the contained liquid as well as subsequent transport through the formed liquid channel and its dispersion by electrostatic forces.²⁹

Fig. 3(a) shows the pictures of the proposed system. The homemade optical microscope (OM) was combined with the QTF-AFM system to directly observe the fluid phenomena on the substrate. The objective lens can be switched from $\times 100$ to $\times 5$ and is used with a charge-coupled device (CCD) camera. The images of the commercial $3 (\pm 0.1) \mu\text{m}$ polystyrene spheres placed on the glass substrate are captured with the OM. These images can be used as a measurement calibration standard for liquid fluids. Fig. 3(b) shows magnified side and front views of the AFM head of Fig. 3(a). The liquid-solution-filled nanopipette is easily aligned on the edge of one of the two prongs of the QTF *via* the fine movement of the XYZ translator by observing with two CCD cameras: one for the x -axis and the other for the y -axis. Then it is glued perpendicularly to the prong with a small amount of epoxy for a shear-mode operation, because the motion of QTF's prongs is parallel to the surface, as shown in the right image of Fig. 3(b). The tip apex of the assembled sensor can directly measure the tip–sample interaction *via* an electrical signal without the use of a cantilever tip that is used in a conventional AFM system. Then the sensor tip approaches the surface while monitoring its surface reflection image and the QTF output signal. The shear-mode QTF-AFM system can only detect the lateral capillary force of the confined nano-water meniscus while excluding other forces such as the van der Waals (vdW) or the electrostatic force, which has a lateral force gradient of zero. Note that the nanopipette/QTF combination is rigid enough to prevent the jump-to-contact problem that occurs in the conventional cantilever-based AFM system when the capillary force of confined water is exerted. The whole and tapered (from tapering start point to tip apex) lengths of the pipette, which can be controlled by varying one of the parameters (pulling power) of the pulling machine, are $\sim 48 \text{ mm}$ and $\sim 3.2 \text{ mm}$, respectively. However, the length of the pipette from the surface to the bottom of the QTF, which is $\sim 100 \mu\text{m}$, must be checked to determine the exact value of the tip's oscillation amplitude. The output current of the QTF was $\sim 0.35 \text{ nA}$ (peak-to-peak), and the estimated dithering amplitude was $\sim 0.06 \text{ nm}$ at the bottom of the QTF. Thus, the oscillation amplitude of the nanopipette apex was $\sim 0.5 \text{ nm}$ according to the geometry of the attached position of the tip. The resonance frequency of the tip was changed to $32\,673.5 \text{ Hz}$ by attachment of the nanopipette, while the quality factor was found to be similar to that of the bare QTFs (~ 6000). In the experiment, the dithering amplitude of the QTF was 0.5 nm , and an electrical current compensation-circuit was used to remove the nonlinear effects of the QTF associated with the stray capacitance of the prongs' electrodes; consequently

the mechanical response of the QTF was well fitted by the linear harmonic oscillator model (Fig. 3(c)).³⁰ A $10 \text{ M}\Omega$ I - V converter was utilized to measure the electrical current through the nanopipette by applying a bias potential between the liquid in the pipette and the substrate. To monitor the behavior of the dispersed liquid *via* the applied electric field, a thin

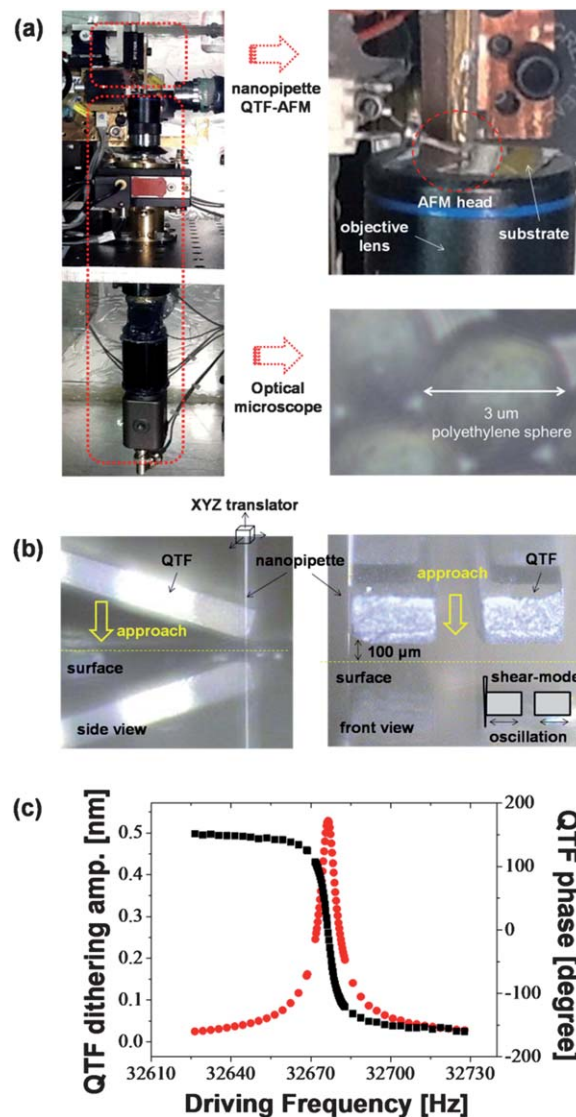


Fig. 3 Photographs and quality factor of the OM built in the combined nanopipette/QTF-AFM system. (a) The OM is placed under the QTF-AFM system to directly monitor the fluidic phenomena on the substrate. The captured OM images of $3 \mu\text{m}$ polystyrene spheres placed on the glass substrate are used to calibrate the length scale of items in the images. (b) Magnified side and front views of the AFM head in (a). The nanopipette is attached perpendicularly to the edge of a prong of the QTF, which is oscillated laterally by the XYZ translator; the nanopipette is guided close to the surface by monitoring simultaneously its surface reflection image and the QTF output signal. (c) The frequency response of the amplitude (\bullet) and phase (\blacksquare) of the nanopipette-attached QTF, which is used as a harmonic oscillator force sensor. Attaching the nanopipette to the QTF shifts the original resonance frequency of the sensor from $32\,763.8 \text{ Hz}$ to $32\,673.5 \text{ Hz}$, and the quality factor is high enough for the measurements (~ 6000).

semitransparent layer of gold (of 20 nm thickness) was sputtered onto a clean hydrophilic mica substrate. Since both temperature and humidity fluctuations significantly influenced the results, we designed a double-chamber setup to maintain constant

temperature (22 ± 0.1 °C) and relative humidity ($50.1 \pm 0.2\%$) within the experimental requirements (thermal drift of ~ 0.3 pm s^{-1}); this was achieved by inserting an acrylic chamber inside a Faraday cage, which shields against electromagnetic noise to

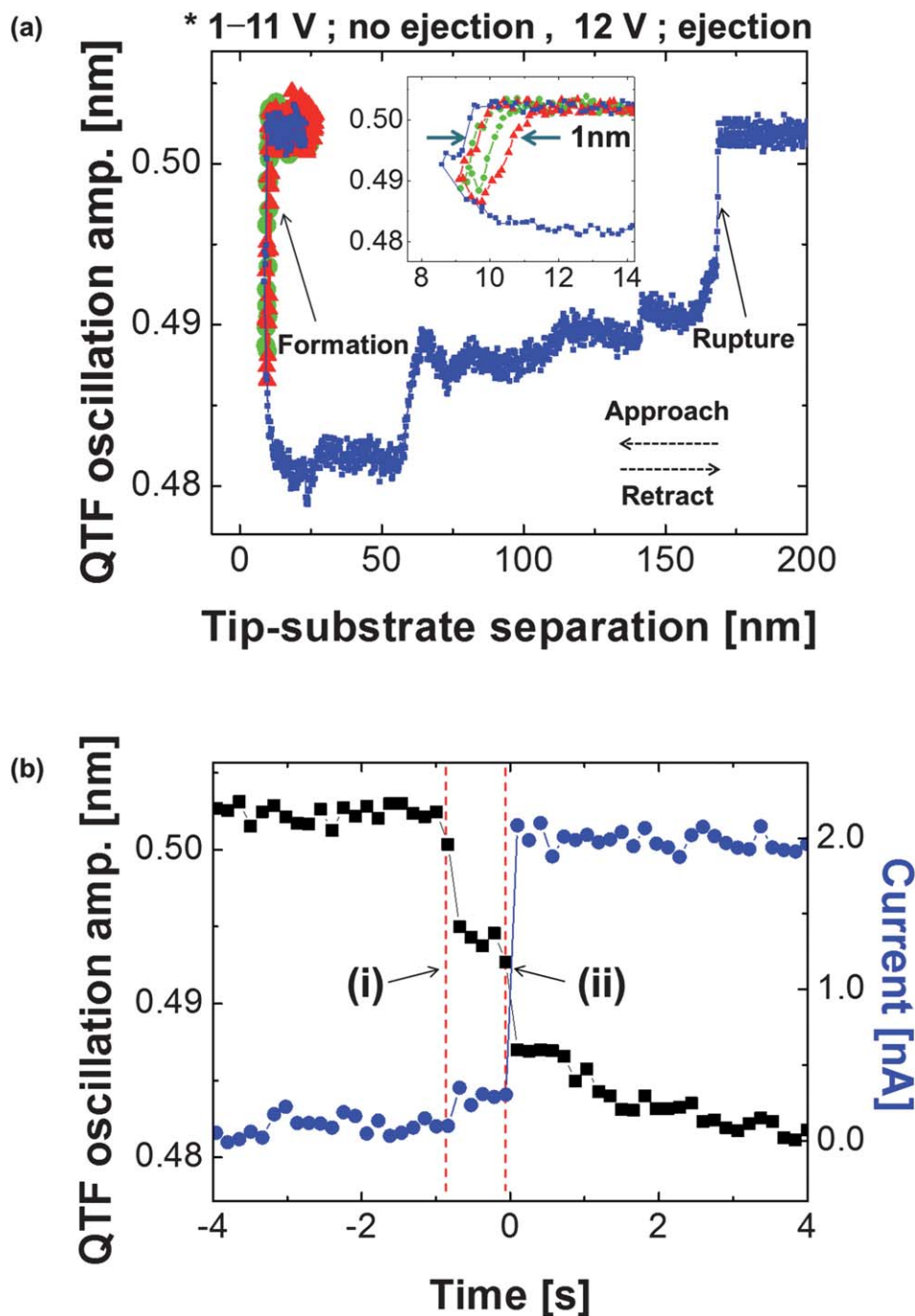


Fig. 4 QTF-AFM signals for the liquid ejection. (a) Approach–retraction curves of the 30 nm aperture nanopipette showing the change of the oscillation amplitudes of the QTF as a function of the tip–substrate separation. When the free oscillation amplitude decreases by a few percent, which results from the water-bridge formation, the tip immediately retracts away from the surface, and finally the water meniscus is ruptured. At 11 V (▲) and below (●), there is no indication of liquid ejection as evidenced by the rupture of the water meniscus over a retraction distance of less than 1 nm (see inset). At 12 V (■), however, a striking difference was observed. The water meniscus ruptured at ~ 161 nm, which indicates the extrusion of the inside liquid (here, the lines connecting the data points are to help guide the eye). (b) Measured QTF sensor signal (■) and electrical current (●) at the moment of formation. After the capillary-condensed water was formed between the aperture rim of the nanopipette and the substrate (i), the liquid inside of the pipette was attracted to the condensed water by an applied electric field (ii). The time difference between these two events (~ 0.9 s) indicates that the formation of the confined water-bridge plays a key role in the ejection of the inside liquid.

isolate the outer and inner environments. In addition, the entire system was supported by spring wires on a commercial anti-vibration optical table to minimize the vibration noise.

Results and discussion

Liquid ejection through the nanoaperture

Fig. 4(a) shows each cycle of the approach–retraction curves, which are typically used in dynamic force spectroscopy, obtained at bias potentials with stepwise increments of 1 V with a 30 nm aperture pipette. When the oscillation amplitude of the QTF decreases by a few percent, as a result of the formation of the confined nano-water due to the capillary condensation, the tip immediately retracts away from the surface, and finally the water meniscus is ruptured. Notice that determination of the exact formation position from the surface and volume of the water bridge, which may follow the Kelvin equation, can be varied by several experimental and environmental factors, such as the apex size of the tip, relative humidity and temperature, the last two of which are controlled by the double-chamber system in this experiment. For example, the rupture distance, effective elasticity and damping of confined water are increased by increasing the relative humidity. However, it is not a relevant issue in this paper, even though it is another important experimental challenge. Up to 11 V, the curves show no discernible difference and are similar to those obtained with no applied electric field. In this case, the rupture of the water bridge was observed about 1 nm from the formation position of the capillary-condensed water meniscus,

and the oscillation amplitude of the QTF decreased slightly, indicating no appreciable ejection of the liquids even in the presence of the confined water meniscus near the apex of the nanopipette (here, the signals with the green circles are the averaged results from 1 V to 10 V). Above 12 V (the critical potential), however, the liquid inside the nanopipette became connected to the water meniscus because of the attractive electrostatic force and started to flow through the meniscus. As a result, the QTF signal decreased, and the corresponding rupture occurred at a substantially elongated distance (~ 161 nm), indicating the extrusion of the liquid from the nanoaperture. Fig. 4(b) shows a magnified version of the QTF sensor signal and the electrical current at the moment of the formation of capillary-condensation and the connection between the water and the liquid in the pipette. It looks like a phase transition. After the capillary-condensed water was formed between the aperture rim of the nanopipette and the substrate in Fig. 4(b)(i), the liquid inside the pipette was attracted and connected to the condensed water by the applied electric field in Fig. 4(b)(ii). Finally, the well-formed nanoscale free-standing liquid acts as a nanoscale fluid channel. These nanofluidic behaviors present clear evidence of the field-induced ejection and transport of the liquid inside the nanopipette through the free-standing liquid meniscus, which acts as a nanochannel. Once the nanochannel is formed, the flow continues by the electro-osmosis effect exerted by the significantly occupied electric double layer (EDL) on the inside wall of the nanopipette's cross-section. The flow rate of the system can be influenced by the thickness of the EDL associated with the applied electric field. Analysis of the field distribution near the

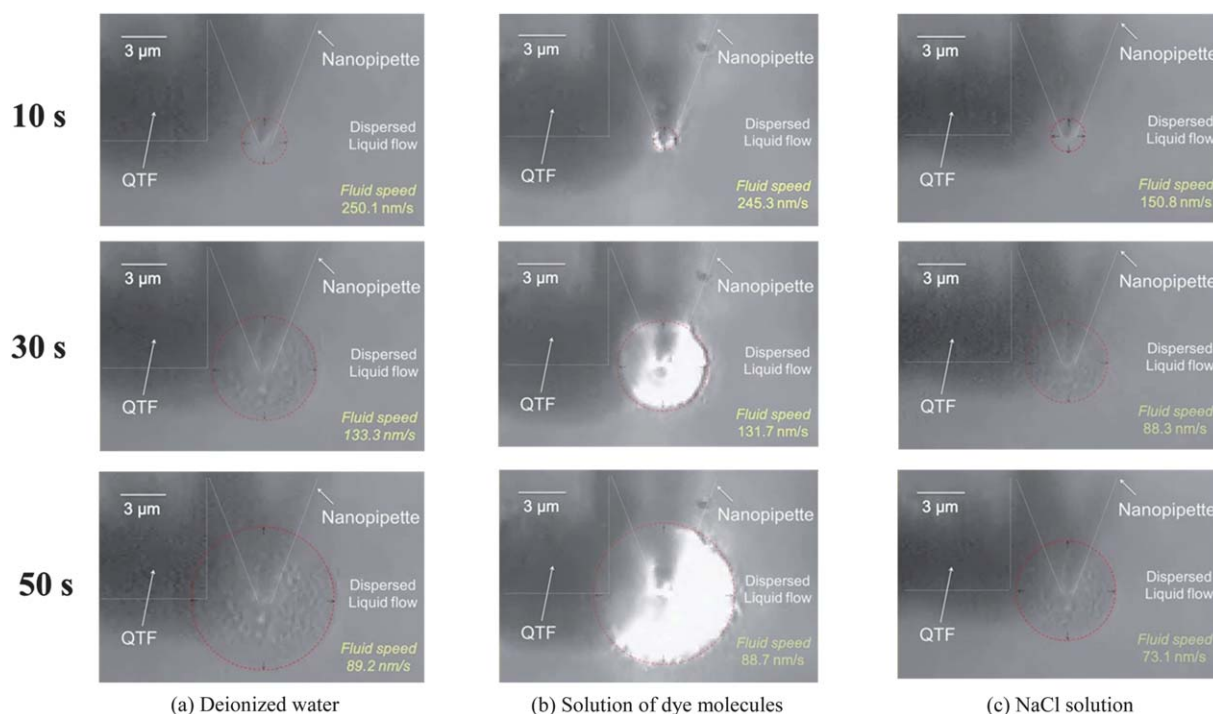


Fig. 5 Three liquid solutions [(a) deionized water (see Movie 1, ESI†), (b) a solution of dye molecules (see Movie 2, ESI†) and (c) a 0.1 M NaCl solution (conductivity of $1.032 \Omega \text{ m}$) (see Movie 3, ESI†)] were studied and their nanofluidic characteristics were measured *in situ* by an optical imaging system. Optical images of the ejected and transported liquids being dispersed on the Au-coated quartz substrate were obtained at intervals of 10 s. The measured fluid speeds of the deionized water and the dye solution were similar but still faster than that of the NaCl solution. A bias potential of 12 V was used for three liquid solutions.

aperture of the nanopipette with the finite element method (FEM) also confirms such a low-field-induced liquid ejection and dispersion onto the substrate through the capillary-condensed water nanomeniscus between the tip and the surface (Fig. S-2 in the ESI†).

Low-volume liquid delivery (nanofluidics)

Well-controlled dispersion on the substrate is one of the essential requirements for the study of nanofluidics and related applications. We analyzed three liquid solutions (deionized water, a solution of dye molecules (rhodamine 6G) representing the molecular liquids and a NaCl solution (0.1 M) representing the ionic solutions) to define the nanofluidic characteristics of the ejected and dispersed liquids. We measured the flow rate of the liquid extracted from the nanoaperture as well as the fluid speed of the liquid during its dispersion on the substrate after being delivered through the liquid nanochannel. The resulting time-dependent dispersion images of the transported liquid on the substrate were directly recorded by a homemade OM built into the AFM.

Fig. 5 displays the *in situ* digital images of each liquid solution taken at 10 s intervals during the dispersion with a bias potential of 12 V. The relative position of the tip above the substrate was fixed when the images of the liquid flow were taken at a rate of 30 frames per second. We determined that, in 50 s, the outward fluid speeds from the centre along one axis (parallel to the surface) (dispersed areas) of the ejected deionized water, dye solution and NaCl solution were $89 \pm 8 \text{ nm s}^{-1}$ ($62 \pm 6 \mu\text{m}^2$), $89 \pm 8 \text{ nm s}^{-1}$ ($61 \pm 6 \mu\text{m}^2$) and $73 \pm 3 \text{ nm s}^{-1}$ ($42 \pm 4 \mu\text{m}^2$), respectively. The results are plotted in Fig. 6(a) with respect to time. While the results of the dye solution were similar to those of the deionized water, the NaCl solution showed appreciable differences. This may be because the electro-osmosis effect is suppressed with decreasing thickness of the EDL due to a shielding effect of the ions near the inner surface of the nanopipette. In addition, the movement of ionic clusters without accompanying water clusters is more active and attractive to the electrodes than the movement of water molecules. We also observed that all three cases exhibited the saturation of both the wetted area and the fluid speed probably due to evaporation³¹ of the finite ejected liquid during dispersion. The evaporation rate following the Kelvin equation was increased by increasing the spread area with respect to time in a closed chamber system with constant temperature ($22 \pm 0.1 \text{ }^\circ\text{C}$) and relative humidity ($50.1 \pm 0.2\%$) in an atmosphere of air at standard pressure. The approximately averaged evaporation rates of each liquid were $\sim 0.35 \text{ mg m}^{-2} \text{ s}^{-1}$ (deionized water), $0.28 \text{ mg m}^{-2} \text{ s}^{-1}$ (dye solution) and $0.46 \text{ mg m}^{-2} \text{ s}^{-1}$ (NaCl solution), respectively. From these results, one can derive the nanofluidic flow rates through the 30 nm aperture when the electrostatic field is applied: $0.79 \pm 0.02 \text{ femtolitre per s (fl s}^{-1}\text{)}$, $0.75 \pm 0.02 \text{ fl s}^{-1}$ and $0.12 \pm 0.01 \text{ fl s}^{-1}$ for deionized water, dye solution and NaCl solution, respectively; these rates are approximately calculated by deriving the spread volume by (1) using the aperture diameter (30 nm), (2) assuming a hydrophilic tip and substrate, and (3) using the rate of evaporation from the surface of liquids. Fig. 6(b) shows the flow rates for deionized water with respect to the bias potential presented for the three different aperture sizes. The linear increase of

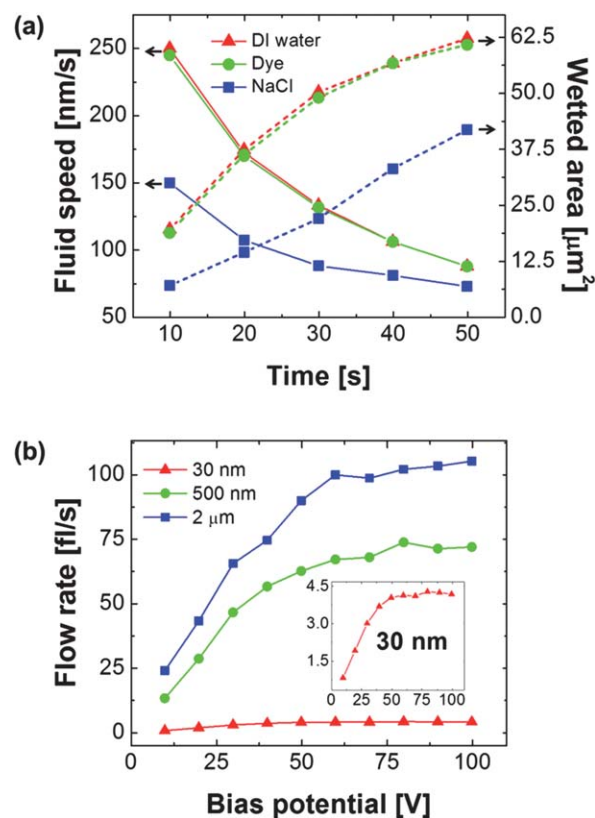


Fig. 6 Nanofluidics with the proposed nanopipette/QTF-AFM system. (a) Plots of the experimental results for the nanofluidic characteristics with respect to time, fluid speeds (solid lines) and wetted areas (dashed lines) for three types of liquids: deionized water (\blacktriangle), a solution of dye molecules (\bullet) and NaCl (\blacksquare). A bias potential of 12 V was used. (b) The flow rates of the ejected liquids (deionized water) with respect to the bias potential for three differing aperture sizes: 30 nm (\blacktriangle ; see inset), 500 nm (\bullet) and 2 μm (\blacksquare), where the linear increase and subsequent saturation are common to all of our observations.

the flow rates may be clearly seen as well as the subsequent saturation occurring above the respective thresholds due to the finite sizes of the apertures. Each pulled pipette was fabricated several times with a typical variation in aperture diameter of $\sim 5\%$, and the measurements of the bias potential dependence were reproducibly performed 10 times. Fig. 6(b) was plotted using averaged values for each size range of apex diameters.

Nanolithography using the nanopipette/AFM

Nanolithography was performed using this well-defined technique. In contrast to the nanofluidic experiment, the Au-coated mica electrode was flipped over. This minimized the effect of the electro-osmosis force inducing continuous liquid ejection, which came from the direct connection of the liquid to the bottom electrode (Fig. 7(a)). The target solution of $5 (\pm 0.3) \text{ nm}$ spherical silver particles was placed inside the pipettes with apertures of 2 μm and 30 nm. It was then patterned on the mica substrate using the proposed method based on the operation of a non-contact mode feedback system. Fig. 7(b) shows the results of the nanolithography (OM and AFM images). After an attolitre-scale volume of solution was ejected, the clusters of 5 nm spheres were

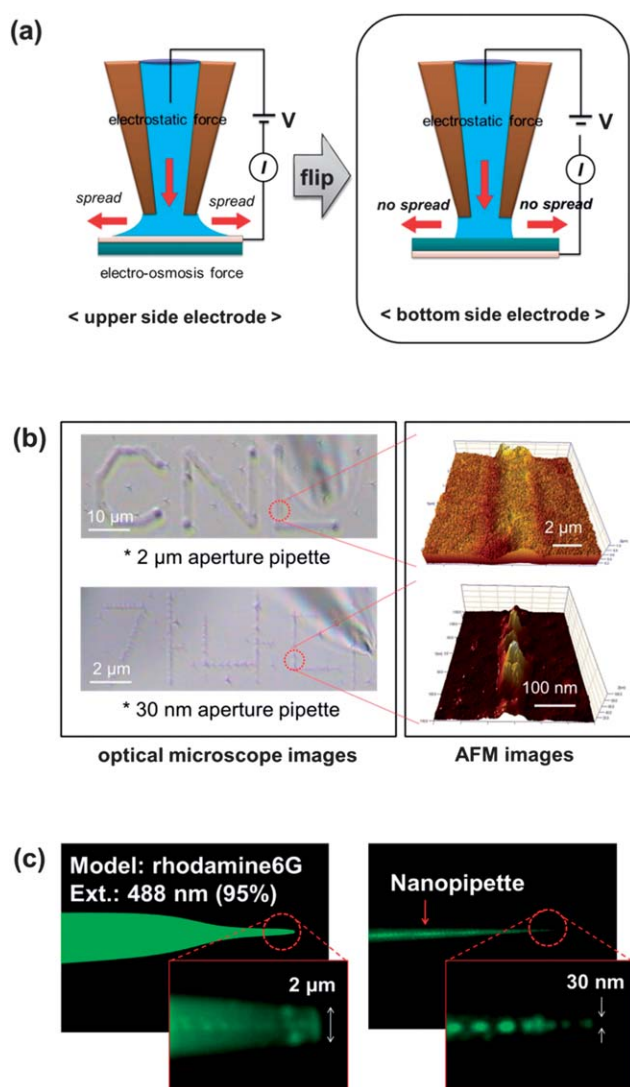


Fig. 7 Nanolithography with the nanoscale liquid ejection based on the QTF-AFM system. (a) Simple schematic of our method to minimize the dispersion of the ejected liquid solution for nanolithography. The Au-coated side of the mica was flipped in order to only use the electro-static force without the electro-osmosis force to suppress the spread of the liquid solution. (b) Results of the nanolithography for both aperture sizes. The line formed by the ejected solution of 5 nm silver spheres was ultimately limited to a width of ~ 80 nm. The OM image was recorded *in situ*, while the AFM images were immediately scanned with the same system after the nanolithography was performed. (c) Fluorescence microscope (MFP-3D-Bio) images of two pipettes having different aperture sizes (2 μm and 30 nm). At the apex of the pipettes, as shown in the insets, the discrete alternating bright and dark strips of clusters of the dye molecules (rhodamine 6G) are consistent with the results of the nanolithography.

nanopatterned with the shape of discrete dots as a result of the evaporation of the liquid, forming tens of nanoscale aggregates, which limited the patterned line widths (~ 80 nm). The mechanism of delivery of the silver particles can be interpreted as the immigration through the inside liquid by the electrophoretic force and attraction of the surface-charged silver particles onto the substrate by an electric field associated with electrophoresis.

To determine the origin of the patterned nanoparticles' shapes, such as the discrete dots, a fluorescence microscope (MFP-3D-Bio Asylum Research Co., magnification factor of 500) was used with dye molecules instead of nanoparticles (due to the diffraction limit of the OM³²) to watch the behavior of molecules near the apex of the nanopipette. The pipettes with apertures of 2 μm and 30 nm were filled with dye molecule (rhodamine 6G) solution, which emits green fluorescence when excited by a 488 nm laser. Moreover, their fluorescence images were obtained in the air, showing that the dye molecules become aggregated and make clusters with an interval of about one cluster distance (explaining the discrete alternating bright and dark strips) in the nanochannel as shown in Fig. 7(c), which may be caused by the interplay of the hydrophobicity of the molecules and the intermolecular electrostatic interactions.³³ These discrete dye molecule clusters are consistent with the results of the nanolithography.

Conclusions

We have demonstrated low-electric-field-induced nanoscale liquid ejection through a nanoaperture pipette (30 nm) *via* the capillary-condensed water meniscus spontaneously formed in the pipette–substrate nanogap. We have investigated its nanofluidic characteristics, such as the fluid speed, flow rate and dispersed area of the ejected and transported nanoscale liquids. With this novel technology, one can extract an extremely small amount of any liquid solution (on the scale of attolitres) or nanosized material (*e.g.*, nanoparticles, nanowires or molecular clusters), and deliver/deposit them selectively onto the substrate under ambient conditions. With such capabilities, the realization of a multicolor-patterning nano-inkjet device may be possible. One can also consider this nanopipette-based method for challenging biological applications, such as the field-induced nanofluidic separation, control and analysis of generic biomolecules.

Acknowledgements

This work was supported by the National Research Foundation of Korea (NRF) grant funded by the Korea government (MEST) (no. 2011-0029541) and the Brain Korea 21. Wonho Jhe acknowledges the support from Center for NanoLiquid and Corey Stambaugh acknowledges support from the National Science Foundation OISE Grant #0853104. Gunn Kim thanks the Priority Research Center Program (grant no. 2012-0005859) of the Korean Government (MEST).

Notes and references

- W. Sparreboom, A. van den Berg and J. C. T. Eijkel, *Nat. Nanotechnol.*, 2009, **332**, 713–720.
- R. B. Schoch, J. Y. Han and P. Renaud, *Rev. Mod. Phys.*, 2008, **80**, 839–883.
- J. C. T. Eijkel and A. van den Berg, *Microfluid. Nanofluid.*, 2005, **1**, 249–267.
- M. Napoli, J. C. T. Eijkel and S. Pennathur, *Lab Chip*, 2010, **10**, 957–985.
- N. Li, S. Yu, C. C. Harrell and C. R. Martin, *Anal. Chem.*, 2004, **76**, 2025–2030.
- S. Lee, R. An and A. J. Hunt, *Nat. Nanotechnol.*, 2010, **5**, 412–416.
- J. Y. Han, F. Jianping and B. S. Reto, *Lab Chip*, 2008, **8**, 23–33.
- F. Paola, M. Valentina, M. Chiara, A. Elena, F. Giuseppe, R. Luca and V. Ugo, *Lab Chip*, 2011, **11**, 2961–2966.

- 9 X. Liang and S. Y. Chou, *Nano Lett.*, 2008, **8**, 1472–1476.
- 10 N. Naguib, H. Ye, Y. Gogotsi, A. G. Yazicioglu, C. M. Megaridis and M. Yoshimura, *Nano Lett.*, 2004, **4**, 2237–2243.
- 11 S. Umehara, N. Pourmand, C. D. Webb, R. W. Davis, K. Yasuda and M. Karhanek, *Nano Lett.*, 2006, **6**, 2486–2492.
- 12 M. G. Schrlau, E. M. Falls, B. L. Ziober and H. H. Bau, *Nanotechnology*, 2008, **19**, 015101–015104.
- 13 M. B. Kim, T. Murray and H. H. Bau, *Nanotechnology*, 2005, **16**, 1317–1320.
- 14 M. G. Schrlau, E. Brailoiu, S. Patel, Y. Gogotsi, N. J. Dun and H. H. Bau, *Nanotechnology*, 2008, **19**, 325102.
- 15 L. Ying, *Biochem. Soc. Trans.*, 2009, **37**, 702–706.
- 16 M. Karhanek, J. T. Kemp, N. Pourmand, R. W. Davis and C. D. Webb, *Nano Lett.*, 2005, **5**, 403–407.
- 17 P. K. Hansma, B. Drake, O. Marti, S. A. Gould and C. B. Prater, *Science*, 1989, **243**, 641–643.
- 18 R. W. Clarke, J. D. Piper, L. Ying and D. Klenerman, *Phys. Rev. Lett.*, 2007, **98**, 198102–198104.
- 19 A. Bruckbauer, P. James, D. Zhou, J. W. Yoon, D. Excell, Y. Korchev, R. Jones and D. Klenerman, *Biophys. J.*, 2007, **93**, 3120–3131.
- 20 M. Hong, J. Bae, K. Kim and W. Jhe, *Appl. Phys. Lett.*, 2000, **77**, 2604–2606.
- 21 P. Kim and C. M. Lieber, *Science*, 1999, **286**, 2148–2150.
- 22 J. Park, M. Hardy, J. Kang, K. Barton, K. Adair, D. K. Mukhopadhyay, C. Lee, M. S. Strano, A. G. Alleyne, J. G. Georgiadis, P. M. Ferreira and J. A. Rogers, *Nat. Mater.*, 2007, **6**, 782–789.
- 23 F. J. Giessibl, *Rev. Mod. Phys.*, 2003, **75**, 949–983.
- 24 F. J. Giessibl, *Appl. Phys. Lett.*, 1998, **73**, 3956–3958.
- 25 H. Choe, M. Hong, Y. Seo, K. Lee, G. Kim, Y. Cho, J. Ihm and W. Jhe, *Phys. Rev. Lett.*, 2005, **95**, 187801–187804.
- 26 M. Lee and W. Jhe, *Phys. Rev. Lett.*, 2006, **97**, 036104.
- 27 M. Lee, H. Noh, Y. Seo, J. Jahng and W. Jhe, *Appl. Phys. Lett.*, 2007, **91**, 023103.
- 28 C. D. Willett, M. J. Adams, S. A. Johnson and J. P. K. Seville, *Langmuir*, 2000, **16**, 9396–9405.
- 29 F. Saija, F. Aliotta, M. E. Fontanella, M. Pochylski, G. Salvato, C. Vasi and R. C. J. Ponterio, *Chem. Phys.*, 2010, **133**, 081104.
- 30 Y. Qin, *Rev. Sci. Instrum.*, 2007, **78**, 063704–063707.
- 31 D. A. Grigoriev and M. J. Edirisinghe, *Appl. Phys. Lett.*, 2002, **91**, 437–439.
- 32 Y. Kuznetsova, A. Neumann and S. R. Brueck, *Opt. Express*, 2007, **15**, 6651–6663.
- 33 D. Sarkar, P. Das, A. Girigoswami and N. Chattopadhyay, *J. Phys. Chem. A*, 2008, **112**, 9684–9691.